

# Evaluation of Imidazole-Based Compounds as Heme Oxygenase-1 Inhibitors

Valeria Sorrenti<sup>1,\*</sup>, Salvatore Guccione<sup>2</sup>,  
Claudia Di Giacomo<sup>1</sup>, Maria N. Modica<sup>2</sup>,  
Valeria Pittalà<sup>2</sup>, Rosaria Acquaviva<sup>1</sup>,  
Livia Basile<sup>3</sup>, Morena Pappalardo<sup>2</sup> and  
Loredana Salerno<sup>2</sup>

<sup>1</sup>Biochemistry Section, Department of Drug Sciences, University of Catania, V.le A. Doria 6, 95125 Catania, Italy

<sup>2</sup>Medicinal Chemistry Section, Department of Drug Sciences, University of Catania, V.le A. Doria 6, 95125 Catania, Italy

<sup>3</sup>Etnalead s.r.l., c/o EtnaBuilding, Scuola Superiore di Catania, University of Catania, V.le A. Doria 6, 95125 Catania, Italy

\*Corresponding author: Valeria Sorrenti, sorrenti@unict.it

**Imidazole-based compounds previously synthesized in our laboratory were selected and reconsidered as inhibitors of heme oxygenase-1 obtained from the microsomal fractions of rat spleens. Most of tested compounds were good inhibitors with IC<sub>50</sub> values in the low micromolar range. Compounds were also assayed on membrane-free full-length recombinant human heme oxygenase-1; all tested compounds were unable to interact with human heme oxygenase-1 at 100 μM concentrations with the exception of compounds 11 and 13 that inhibited the enzyme of 54% and 20%, respectively. The binding of the most active compound 11 with heme or heme-conjugated human heme oxygenase-1 was also examined by spectral analyses. When heme was not conjugated to human heme oxygenase-1, compound 11 caused changes in the heme spectrum only at concentration 50-fold (100 μM) higher than that required to inhibit rat heme oxygenase-1; when heme was conjugated to human heme oxygenase-1, compound 11 was able to form a heme-compound 11 complex also at low micromolar concentrations. To obtain information on the binding mode of the tested compounds with enzyme, docking studies and pharmacophore analysis were performed. Template docking results were in agreement with experimental inhibition data and with a structure-based pharmacophoric model. These data may be exploitable to design new OH-1 inhibitors.**

**Key words:** docking studies, enzymatic and spectral analyses, HO-1 inhibitors, imidazole-based compounds, pharmacophoric model

Received 7 May 2012, revised 26 June 2012 and accepted for publication 30 July 2012

Heme oxygenase (HO) is a microsomal enzyme catalyzing the first, rate-limiting step in degradation of heme, yielding equimolar quantities of carbon monoxide (CO), Fe<sup>2+</sup>, and biliverdin (1). Finally, biliverdin is converted by biliverdin reductase to bilirubin (2), which can be oxidized by cytochrome P450 (CYP450) enzymes (3). Three distinct mammalian HO isoforms (HO-1, HO-2, and HO-3) have been identified, which are the products of different genes (4). HO-1, the inducible 32-kDa isoform, is highly expressed in the liver and spleen, but can be also detected in many other tissues. HO-2 is a constitutively expressed 36-kDa protein, present in high levels in the brain, testes, or endothelial cells. HO-3 was postulated as a 33-kDa protein expressed in different organs, very similar to HO-2, but with much lower catalytic activity (5). The HO system has been demonstrated to have a variety of cellular regulatory actions including anti-inflammatory, anti-apoptotic, anti-proliferative, and vasodilator effects, owing to contributing and complementary effects of each of the metabolites produced (6–9).

Interestingly, expression of HO-1 is usually increased in tumors, compared with surrounding healthy tissues (10–13). It has been reported that the growth of a number of tumors is dependent on HO-1 activity (14). These results support the idea that HO-1 may be a potential target in antitumor therapy. Thus, pharmacologic inhibition of HO-1 has been suggested as a new therapeutic option and potential sensitizer to chemotherapy, radiotherapy, or photodynamic therapy for several tumors (15–18). The efficacy of such treatments has been proven in animal models. Thus, administration of metalloporphyrins such as tin protoporphyrin (SnPP) or zinc protoporphyrin (ZnPPiX) (19,20) significantly suppressed the growth of hepatoma in rats (21), and sarcoma (22) or lung cancer in mice (23). However, owing to the close structural similarity between heme and the metalloporphyrin-HO inhibitors, specificity becomes a problem. In several systems, proteins bind heme and employ it for functions such as regulation of enzyme activity (i.e., of soluble guanylyl cyclase sGC) or as the key component of the active site of an enzyme (i.e., nitric oxide synthase NOS and CYP450). Accordingly, the use of metalloporphyrins to ascribe various physiological roles to the CO/HO system has been the subject of some criticism because they have been shown to affect the activity of both NOS and sGC (24,25). Thus, programs in various laboratories were concerned with the design of HO inhibitors that are not based on the porphyrin nucleus and have the goal of obtaining more selective HO inhibitors.

Vlanakis *et al.* (26–28) and Roman *et al.* (29,30) describe HO inhibitory activity of a series of imidazole-dioxolanes designed basing on the structure of azalanstat (**1**, Figure 1), the first non-porphyrin inhibitor of HO (26). Appropriate synthetic modifications to the

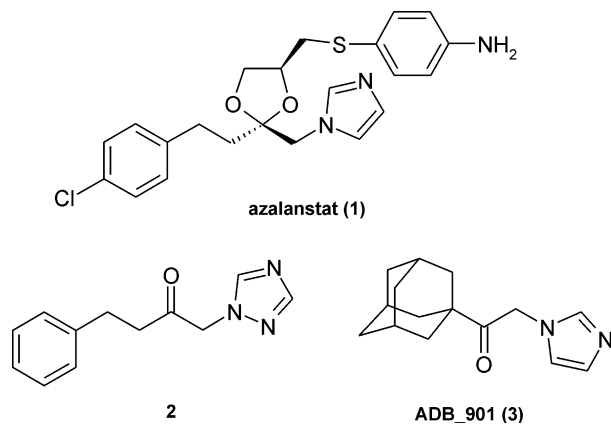


**Figure 1:** Chemical structures of representative literature compounds **1–3**.

structure of **1** lead to the development of imidazole-based analogues having enhanced inhibitory potency for HO-1 over other heme-dependent enzymes (such as sGC and NOS) (31), and an isozyme-dependent HO selectivity (26,27). Representative compounds **1–3** emerged from these studies are depicted in Figure 1.

Rahman *et al.* (32,33) continued to investigate onazole-based HO-1 inhibitors, which act in a non-competitive manner with respect to heme. These studies provided valuable information about the mode of binding of these compounds to HO-1 causing inhibition of heme oxidation. Furthermore, they elucidated the main structural features required for the binding to HO-1. The mechanism through these compounds inhibit heme oxidation is the disruption of an ordered hydrogen-bond network involving Asp140 and, ultimately, displacement of the distal water ligand deemed to be critical for catalysis. Structural characterization by X-ray crystallography of theseazole-based inhibitors in complex with HO-1 (some of them are listed in Figure 1) shows that the main features for binding include coordination with the heme iron of the N-3 nitrogen present in the imidazolyl moiety of the inhibitors, and stabilization by an interaction between hydrophobic groups of the inhibitors and a distal hydrophobic pocket in the heme-binding pocket. It should be noted that all of the structural analyses of inhibitors in complex with HO-1 presented in the above cited studies have been performed using soluble, truncated versions of the protein. The full-length human heme oxygenase (hHO-1) has been recently expressed and purified (34). Characterization of the full-length hHO-1 demonstrated a 2,3-fold greater activity relative to that of the truncated, soluble form, which was increased even further in the presence of lipids. Further analyses suggested an important role of the C-terminal hydrophobic tail in membrane incorporation as well as formation of a high-affinity complex with CYP450 reductase (34–36). Then, the chance that this domain could significantly influence hHO-1 conformation should be taken into account for future design of novel inhibitors.

In recent years, our research group has conducted extensive investigations on a number of imidazole-based compounds designed as NOS inhibitors (37–42). These molecules present an imidazole nucleus separated from a hydrophobic aryl moiety by different spacers such as an ethanone, an alkylene, an ethanol, or an alkoxy

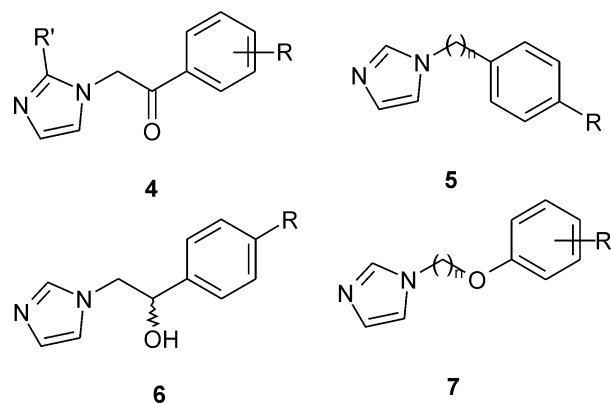


**Figure 2:** General formulae of compounds **4–7**.

chain of different length, giving compounds of general formulae **4–7** (Figure 2). The majority of these compounds possesses the two key features required for the binding to HO-1 (i.e., the N-3 imidazole nitrogen and a hydrophobic moiety); consequently, they might constitute a collection of imidazole-based compounds useful to select novel inhibitors of this enzyme.

A virtual screening for the above-mentioned imidazole collection using the X-ray structure (PDB\_ENTRY = 3CZY) of the HO-1 co-crystallized with 1-(adamantan-1-yl)-2-(1*H*-imidazol-1-yl)ethanone AD8\_901 (**3**, Figure 1) was undertaken to select new potential inhibitors. From this screening, a group of compounds showed interesting binding energies; six of them (**8–13**, Figure 3), further characterized by low or no effect on NOS (37,40,42) and CYP450 activities (data not shown), were chosen for biological and molecular modeling studies. Thus, compounds **8–13** were tested *in vitro* to evaluate their inhibitory activity on HO-1. Enzyme inhibition assays were performed on HO-1 obtained from rat spleen as the microsomal fraction and on full-length recombinant hHO-1. The binding of the tested compounds to heme-conjugated hHO-1 was additionally examined by spectral analyses. Moreover, to rationalize the binding mode, compounds **8–13** were the object of

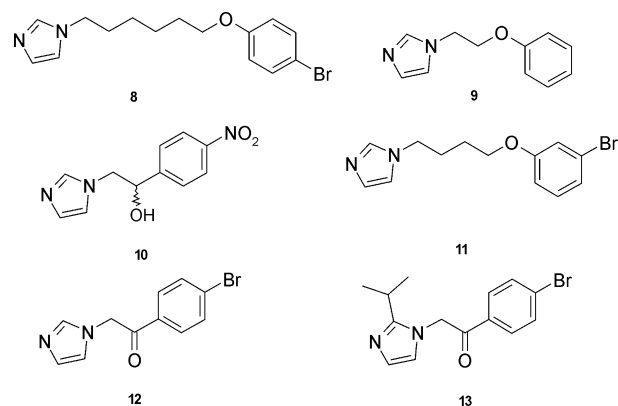


**Figure 3:** Chemical structures of tested compounds **8–13**: **8**: 1-[6-(4-Bromophenoxy)hexyl]-1*H*-imidazole; **9**: 1-(2-Phenoxyethyl)-1*H*-imidazole; **10**: 2-(1*H*-imidazol-1-yl)-1-(4-nitrophenyl)ethanol; **11**: 1-[4-(3-Bromophenoxy)butyl]-1*H*-imidazole; **12**: 1-(4-Bromophenyl)-2-(1*H*-imidazol-1-yl)ethanone; **13**: 1-(4-Bromophenyl)-2-[2-(1-methylethyl)-1*H*-imidazol-1-yl]ethanone.

molecular docking studies and of the generation of a pharmacophoric model by the use of LIGAND SCOUT software (Inte:Ligand Software-Entwicklungs und Consulting GmbH, Vienna, Austria).

## Methods and Material

### Biological studies

#### Preparation of spleen microsomal fractions

HO-1 was obtained from rat spleen as the microsomal fraction prepared by differential centrifugation; the dominance of HO-1 protein in the rat spleen has been well documented (4,31,43,44). These particular microsomal preparations were selected to use the most native (i.e., closest to *in vivo*) forms of HO-1. Spleen (Sprague–Dawley rats) microsomal fractions were prepared according to the procedure outlined by Ryter *et al.* (45). The experiments reported in the present paper complied with current Italian law and met the guidelines of the Institutional Animal Care and Use Committee of University of Catania (Italy). The experiments were performed in male Sprague–Dawley albino rats (150 g body weight and age 45 days). They had free access to water and were kept at room temperature with a natural photoperiod (12-h light/12-h dark cycle). For measuring HO-1 activity, each rat was killed and its spleen was excised and weighed. A homogenate (15%, w/v) of spleens pooled from four rats was prepared in ice-cold HO-homogenizing buffer (50 mM Tris buffer, pH 7.4, containing 0.25 M sucrose) using a Potter-Elvehjem homogenizing system with a Teflon pestle. The microsomal fraction of rat spleen homogenate was obtained by centrifugation at 10 000×g for 20 min at 4 °C, followed by centrifugation of the supernatant at 100 000×g for 60 min at 4 °C. The 100 000×g pellet (microsomes) was resuspended in 100 mM potassium phosphate buffer, pH 7.8 containing 2 mM MgCl<sub>2</sub> with a Potter-Elvehjem homogenizing system. The rat spleen microsomal fraction was divided into equal aliquots, placed into microcentrifuge tubes, and stored at –80 °C for up to 2 months. Protein concentration of the microsomal fraction was determined by Lowry method (46).

#### Preparation of biliverdin reductase

Liver cytosol has been used as a source of biliverdin reductase (BVR). Rat liver was perfused through the hepatic portal vein with cold 0.9% NaCl, and then it was cut and flushed with 2 × 20 mL of ice-cold PBS to remove all of the blood. Liver tissue was homogenized in three volumes of solution containing 1.15% KCl w/v and Tris buffer 20 mM, pH 7.8 on ice. Homogenates were centrifuged at 10 000×g, for 20 min at 4 °C. Supernatant was decanted and centrifuged at 100 000×g for 1 h at 4 °C to sediment the microsomes. The 100 000×g supernatant was saved and then stored in small amounts at –80 °C after its protein concentration was measured.

#### Measurement of HO-1 enzymatic activity in microsomal fraction of rat spleen

The HO-1 activity was determined by measuring the bilirubin formation using the difference in absorbance at 464–530 nm as described by Ryter *et al.* (45). Reaction mixtures (500 μL) consisted

of 20 mM Tris–HCl, pH 7.4 (1 mg/mL) microsomal extract, 0.5–2 mg/mL biliverdin reductase, 1 mM NADPH, 2 mM glucose 6-phosphate (G6P), 1 U G6P dehydrogenase, 25 μM hemin, and 10 μL of DMSO (or the same volume of DMSO solution of test compounds to a final concentration of 100, 10, and 1 μM). HO inhibitor SnPP (Frontiers Scientific-Porphyrin Products Inc., Logan, UT, USA) was employed as reference compound. Incubations were carried out for 60 min at 37 °C in a circulating water bath in the dark. Reactions were stopped by adding one volume of chloroform. After recovering the chloroform phase, the amount of bilirubin formed was measured with a double-beam spectrophotometer as OD<sub>464–530</sub> nm (extinction coefficient, 40 mm/cm for bilirubin). One unit of the enzyme was defined as the amount of enzyme catalyzing the formation of 1 nmol of bilirubin/mg protein/h.

#### Recombinant HO-1 assay

Recombinant HO-1 (Assay Designs, Ann Arbor, MI, USA) (0.1 μM) preparations were added in 100 mM phosphate buffer pH 7.4, containing 2 mM MgCl<sub>2</sub>, 1 mM G6P and 0.1 U G6P dehydrogenase, and biliverdin reductase in total 100 μL volume. Reaction was initiated by addition of 0.1 mM NADPH and bilirubin produced in the assay was measured by difference in absorbance at 464 and 530 nm (40 mm/cm) over 3 min at 37 °C. One unit of the enzyme was defined as the amount of enzyme catalyzing the formation of 1 nmol of bilirubin/nmol HO-1/h.

#### Spectral analyses

The absorption spectra of compound **11**-heme complex were recorded on a double-beam spectrophotometer according to the method outlined by Kinobe *et al.* (47). Different concentrations of compound **11** (10–100 μM) and a solution of 17 μM heme in 40% v/v DMSO and 20 mM HEPES buffer, pH 7.4, at 25 °C were used. Under these conditions, heme exists as a monomer with characteristic absorption spectra between 350 and 700 nm (48,49).

Heme-conjugated HO-1-compound **11** absorption spectra were recorded using recombinant HO-1 (Assay Designs) combined with a 1.2:1 molar ratio of hemin; this complex was rocked at 4 °C for 20–30 min, and stored at –20 °C. The excess heme was removed by passage over a PD-10 size-exclusion column (Amersham Biosciences) that had been equilibrated with 20 mM potassium phosphate (pH 7.4). Protein concentration was determined by absorbance ( $\epsilon_{405} = 140$  mM/cm). Inhibitor binding was determined by incubation of 0.1 μM heme-conjugated HO-1 with different concentrations of compound **11** (0, 10, 100 μM) in 20 mM potassium phosphate buffer (pH 7.4) for 5 min at room temperature. Spectra were recorded between 300 and 700 nm at 1 nm intervals.

#### Molecular modeling studies

##### Docking studies

All the molecular modeling studies were carried out on a desktop PC, Intel® Core™ i7 960 3.20 GHz, RAM 16.5 GB operating under LINUX (Ubuntu 11.04), using the software MOLEGRO VIRTUAL DOCKER (MVD version 4.3) (50).<sup>a</sup>

Compounds **8–13** were docked into the active site (Met34, Phe37, Val50, Leu54, Arg136, Gly139, Asp140, Ser142, Gly143, Leu147, Phe162, Phe166, Phe214) of the hHO-1 (PDB\_ENTRY = 3CZY). Binding residues Met34, Phe37, Leu54, Arg136, Gly139, Asp140, Leu147 (28,32,33) were considered flexible during the docking simulation. The backbone was kept rigid, but the torsional angles in the side-chains were allowed to change. Sybyl.mol2 files were built using the server ProdrG (<http://davapc1.bioch.dundee.ac.uk/prodrG/>) (51). The X-ray structure (PDB\_ENTRY = 3CZY) of the HO-1 co-crystallized with compound **3**, Figure 1 (32), was used for the docking. Three protocols were used: semi-flexible docking with template (*template docking*), standard semi-flexible docking, and flexible docking, as implemented in MVD. Template docking can be used when the 3D conformation of a ligand is available. The seemingly bioactive conformation of compound **3** as extracted from its complex with HO-1 (PDB\_ENTRY = 3CZY) (32) was used to create a template acting as guide in the docking calculation. The template is implemented as a scoring function rewarding poses similar to the specified pattern (*Similarity Score*), in addition to the MolDock Score. MolDock Optimizer was chosen as the search algorithm and 50 iterations were carried out. Poses were clustered using 1.5 Å as root mean square deviation (RMSD) threshold. Default parameters were used for both of the scoring function and the search algorithm.

The Rerank Score and the Data Analyzer Tool as implemented in MVD were also applied to further refine the results. The former tool provides a good estimation of the strengths of interaction without taking into account contributes such as entropy. This score might be successful in ranking poses of the same ligand but it might fail in ranking poses of structurally different ligands.

### Pharmacophoric model

The software used for the construction of the pharmacophoric models is LIGAND SCOUT, a software with an automated method for pharmacophoric model generation using a structure-based approach (52). LIGAND SCOUT is a tool that allows the automatic construction and visualization of 3D pharmacophores from structural data of macromolecule/ligand complexes. Ligand Scout algorithm chemical features include hydrogen-bond donors (HBD) and acceptors (HBA) as directed vectors (optionally including projected points). Positive (P) and negative (N) ionizable regions as well as lipophilic areas (AR) are represented by location spheres. The generated pharmacophore is based on a set of rules for hydrogen bonding, charge, and lipophilic interactions. This pharmacophore represents a model that is universal and comparable but still specific to reflect a certain mode of action. In fact, this method is able to present the interactions of a ligand to the target protein in a very specific way, and hence, it is capable of providing selective and specific pharmacophoric models. Moreover, to increase the selectivity, the Ligand Scout model includes spatial information regarding areas inaccessible to any potential ligand thus reflecting possible steric restrictions. In particular, excluded volume spheres placed in positions that are sterically forbidden are automatically added to the generated pharmacophoric model. Shared and merged structure-based pharmacophoric models were generated. These models consist of some features that should be essential for the interaction and the biological activity of the drugs. A shared pharmacophoric model shows only the features that

are in common with the ligands taken into account, while the merged one is formed by 'combining' all the features of each ligand.

The Ligand Scout query was generated taking into account the training set molecules **8–13**. The main residues involved in the construction of the query were Met34, Phe37, Leu54, Arg136, Gly139, Asp140, Leu147, as shown in Figure 4.

With regard to structure-based model, superimposed features were deleted and the applied tolerance (from 3.5 to 5.5 Å) for some repeated hydrophobic features was increased of 0.15 Å to render less restrictive the model. Non-essential chemical features and exclusion volume spheres were removed; five of these features (Figures 5 and 6) were marked as optional (the features that are not matched by more than 20% of the molecules) to spread the sensitivity of the model. For the ligand-based query, the molecules were minimized using the MMFF94 energy (53) with 163 iterations and an energy cutoff of 20 299 Kcal/mol.

The forcefield considers the free molecule energy minimization. The merged model was generated after the alignment of the training set. To perform the alignment, the most active compound **11** was selected as the reference molecule. A ligand-based design generates the query considering one conformation of the most active compound. For this reason, it could be less accurate in comparison

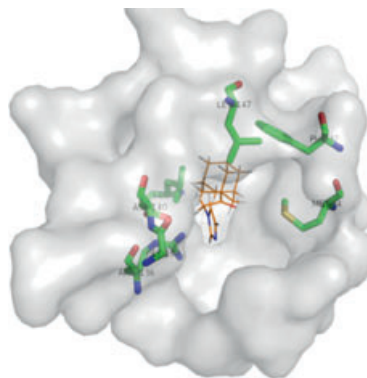


**Figure 4:** Residues involved in the building of the query. Compound **3** is represented in orange lines.

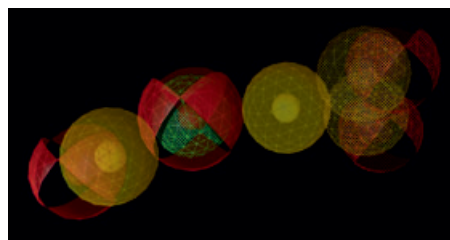


**Figure 5:** Representation of the HO-1 pharmacophoric model with the *optional features*: four hydrophobic features (yellow spheres), four hydrogen bond acceptor (HBA, red spheres), and 1 optional hydrogen bond donor (HBD green sphere) are shown. The optional features are represented by squared spheres.

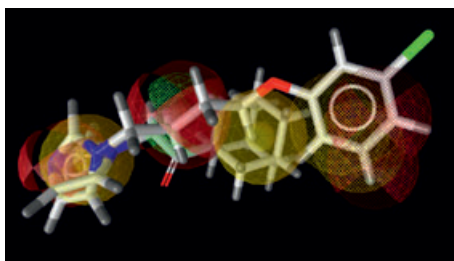


**Figure 6:** Superposition of compounds **3** and **11** fitted with the merged pharmacophore.

with the structure-based one. With the ligand-based approach, the main interactions ('features') that are common to all the molecules of the training set are depicted owing to the similarity among this specific set of molecules (Figure 7). Each orientation of a conformer results from a different mapping and alignment of pharmacophore features on the ligand to the query features. The number of returned results can be filtered. Alignments were kept when conformations mapped with their pharmacophore features within a max RMSD of 3.00 Å. Alignments above the threshold of 3.00 Å were discarded and only 20 results were finally considered to get a consensus pharmacophore. The two different approaches were compared and no significant differences were in the queries. For the ligand-based modeling approach, new conformers were generated, setting 'pharmacophore fit' as scoring function, a RMS threshold of 0.4, and a maximum number of conformations of 500. The degree of mapping was expressed in terms of pharmacophoric score (Table 1).

## Results and Discussion

### Biological studies

Compounds **8–13** were tested to evidence their ability to inhibit HO-1 using an *in vitro* assay. HO-1 was obtained from rat spleen as the microsomal fractions prepared by differential centrifugation.

These particular microsomal preparations were selected to use the most native (i.e., closest to *in vivo*) forms of HO-1, that is, those being most relevant to anticipate whole-animal studies. Precedent studies employed pure forms of HO-1 that were membrane-free and truncated (54,55). Recently, a full-length 32-kDa stable form of HO-1 that has a higher affinity for CYP450 when compared with the truncated 30-kDa species has been purified, suggestive of an important role for the C-terminal region in the CYP450-HO-1 interaction. It was showed that the C-terminal region present on HO-1 influences both membrane incorporation and the formation of a high-affinity complex between full-length HO-1 and endoplasmic reticulum resident enzymes such as CYP450 (34,35). To highlight the ability of our compounds to inhibit the membrane-free full-length recombinant HO-1, we employed also this enzymatic form.

Microsomal rat spleen HO-1 activity without inhibitors was  $2.42 \pm 0.1$  nmol bilirubin/1 h/mg prot. Inhibitory potency is expressed as  $IC_{50}$ . The data obtained using this series of imidazole derivatives revealed general good inhibitory activity of HO-1.

Compounds **8–12** showed  $IC_{50}$  values in the micromolar range. The most active of tested compounds were **11** and **12** with  $IC_{50}$  values = 2.1 and 2.5  $\mu$ M, respectively. Compound **13** was found to exhibit the lowest potency, with  $IC_{50}$  values >100  $\mu$ M. The significantly reduced inhibitory potency of compound **13** respect its structural analogue **12** showed that a substituent on the imidazole moiety reduces substantially its interaction with HO-1 (Table 2).

To highlight a possible interaction between tested compounds and a membrane-free full-length recombinant HO-1, we measured the activity of this enzymatic form in absence of CYP450 reductase. As reported by Huber *et al.* (36), free full-length recombinant HO-1 activity is 2,3-fold increased from the truncated soluble 30-kDa HO-1; moreover, free full-length recombinant HO-1 was active also in absence of CYP450 reductase whereas truncated HO-1 was inactive. These experimental data suggest that the C-terminal 23 amino acids present on full-length HO-1 are essential for maximal catalytic activity. In our experimental conditions, free full-length HO-1 activity

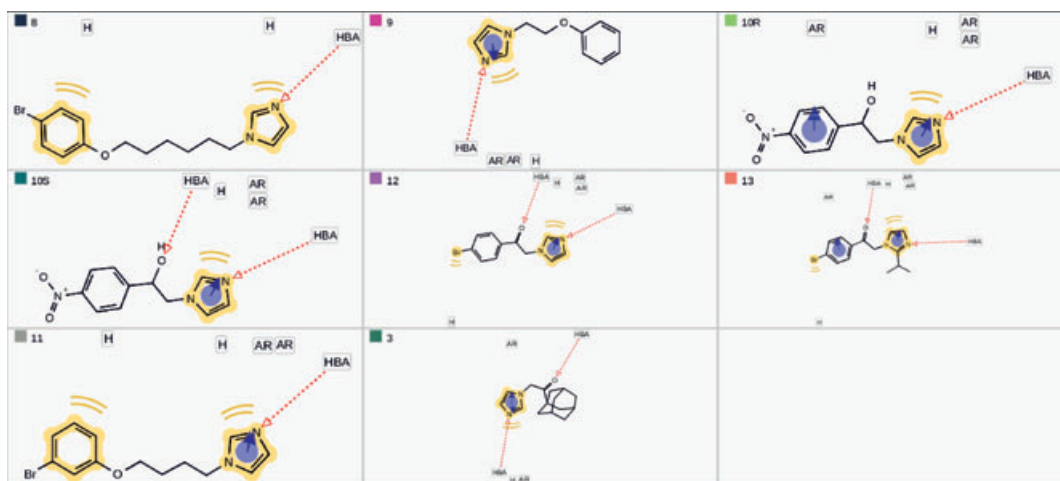


**Figure 7:** Analysis of the most representative common features obtained through a ligand-based approach. The AR features refer to aromatic rings; the HBA features are represented with a red scroll. The optional features are represented by squared features.

**Table 1:** Pharmacophoric scores obtained by the ligand-based approach

Compound	Conformers	Pharmacophoric score	MMFF94			
			strain energy	Ring	Acceptor	Donor
<b>8</b>	500	56.22	621.4951	2	2	0
<b>9</b>	90	45.80	245.1133	2	2	0
<b>10R</b>	35	58.87	121.2577	2	4	1
<b>10S</b>	61	57.75	91.5059	2	4	1
<b>11</b>	500	56.59	33.1492	2	2	0
<b>12</b>	121	63.01	55.12952	2	2	0
<b>13</b>	184	66.29	664.6370	2	2	0
<b>3</b>	32	36.85	39.46164	4	2	0

was  $30 \pm 2$  nmol bilirubin/1 h/1 nmol HO-1. All tested compounds were unable to interact with recombinant HO-1 at 100  $\mu$ M concentrations with the exception of compounds **11** and **13** that showed a capacity to inhibit enzymatic activity of 54% and 20%, respectively (Table 3).

Results obtained in the present study allow us to show that, even if free full-length recombinant HO-1 activity is higher than activity of recombinant truncated form, the crude microsomal spleen form of HO-1, as reported by Vukomanovic *et al.* (56), was more susceptible to inhibition than was the truncated or full-length recombinant form. This difference may be attributed to the extra amino acids present in the full-length enzyme, suggestive of an important role for the C-terminal region that influences both membrane incorporation and the formation of a high-affinity complex between full-length HO-1 and CYP450. The capacity of compound **11** to inhibit

**Table 2:** Compounds tested for microsomal rat spleen HO-1 inhibition

Ligand	IC <sub>50</sub> ( $\mu$ M)
<b>8</b>	10
<b>9</b>	28
<b>10<sup>a</sup></b>	10
<b>11</b>	2.1
<b>12</b>	2.5
<b>13</b>	>100
<b>SnPP</b>	0.58

<sup>a</sup>Compound **10** was experimentally assayed as a racemate.

**Table 3:** Compounds tested for free full-length recombinant HO-1 inhibition

Ligand	% inhibition (100 $\mu$ M)
<b>8</b>	0
<b>9</b>	0
<b>10<sup>a</sup></b>	0
<b>11</b>	54
<b>12</b>	0
<b>13</b>	27
<b>SnPP</b>	100

<sup>a</sup>Compound **10** was experimentally assayed as a racemate.

at the same concentration, particularly the crude microsomal spleen form of HO-1 rather than full-length recombinant form, allows us to evidence that it might interact not only with protein HO-1 but with the complex heme/HO-1/CYP450. Compound **13**, differently from compound **11**, is able to inhibit weakly, at the same concentration, both the crude microsomal spleen form of HO-1 and full-length recombinant form. This result allows us to evidence that it might interact only with protein HO-1 rather than with the complex heme/HO-1/CYP450. As compound **11** resulted the most interesting among tested compounds, we selected it to study its capacity to interact with heme. The HO-1 itself is not a heme protein and forms a 1:1 complex with heme with absorbance spectral characteristics similar to that of methemoglobin. HO-1 employs heme as both prosthetic group and substrate. The binding of the most active compound **11** with heme or heme-conjugated recombinant HO-1 was examined by spectral analyses.

In the absence of heme, recombinant HO-1 or compound **11** did not exhibit any characteristic spectra (Figure 8). In the absence of inhibitor, heme gave a characteristic absorption spectrum of high-spin ferric complexes assuming a five-co-ordinate structure. A Soret band absorption at 401 nm was observed (Figure 9). There were no observable spectral changes when compound **11** (10  $\mu$ M, final concentration) was added to heme (Figure 9A). Whereas in the presence of compound **11** at the concentration of 100  $\mu$ M in the mixture, there was a marked decrease in the absorption maximum and a shift to 412 nm of the Soret band (Figure 9B) characteristic of hexacoordinate ferrous form (low spin).

These observations, according to Kinobe *et al.* (48), revealed that the concentration of compound **11** that was required to cause changes in the heme spectrum was in the order of 50-fold (100  $\mu$ M) higher than that found to inhibit rat HO-1 activity *in vitro* and are not consistent with compound **11** forming a complex with heme at low micromolar concentrations. In the absence of inhibitor, the heme-bound HO-1 gave a characteristic spectrum with a Soret peak at 401 nm (Figure 10). With increasing amounts of compound **11** (10–100  $\mu$ M), concentrations at which HO-1 was presumed to have been saturated with inhibitor, the Soret peak shifted to longer wavelengths up to 412 nm. The shift in the Soret peak was suggestive of a change in the heme environment and, thus, putative binding of the inhibitor (Figure 10A,B). These results revealed that when heme is bound to HO-1, compound **11** was able to form a complex with heme also at low micromolar concentrations.

Our results, according to Rahman *et al.* (33), show that the imidazole group of the inhibitor serves as an anchor with the N-3 coordinating with the heme iron atom to result in a hexacoordinate heme iron. The capacity of compound **11** to interact, at low micromolar concentrations, only with heme bound to HO-1 might be in agreement with its selectivity versus HO-1 rather than other heme enzymes such as NOS or CYP450.

### Docking studies

The best docking results (Table 4) were obtained applying a template docking protocol and the predicted ranking was similar to the experimental one. The similarity score of compound **3** was near the

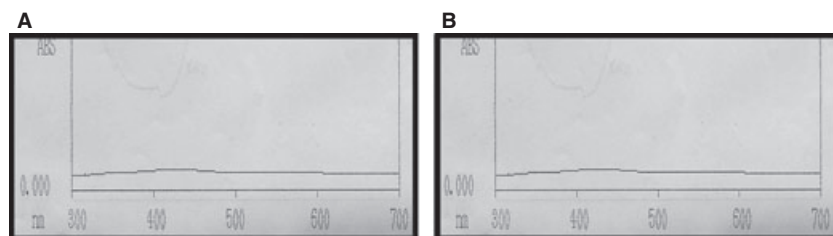


**Figure 8:** (A) Absorption spectrum of 0.1  $\mu\text{M}$  full-length recombinant HO-1; (B) absorption spectrum of 100  $\mu\text{M}$  compound **11**.

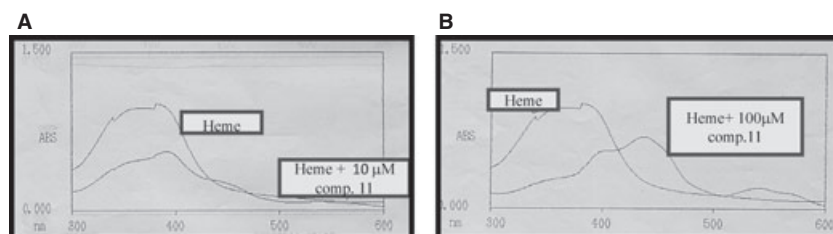


**Figure 9:** (A) Absorption spectra of 0.1  $\mu\text{M}$  heme and 0.1  $\mu\text{M}$  heme + 10  $\mu\text{M}$  compound **11**; (B) absorption spectra of 0.1  $\mu\text{M}$  heme and 0.1  $\mu\text{M}$  heme + 100  $\mu\text{M}$  compound **11**.

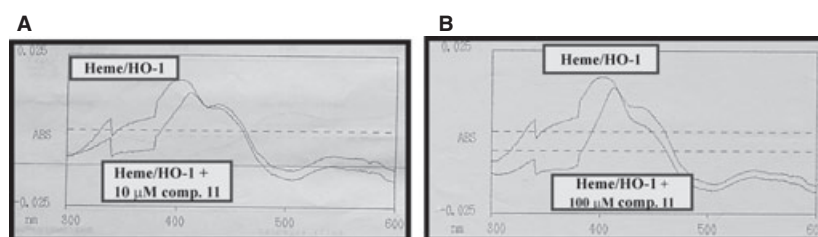


**Figure 10:** (A) Absorption spectra of 0.1  $\mu\text{M}$  heme-conjugated recombinant HO-1 and 0.1  $\mu\text{M}$  heme-conjugated recombinant HO-1 + 10  $\mu\text{M}$  compound **11**; (B) absorption spectra of 0.1  $\mu\text{M}$  heme-conjugated recombinant HO-1 and 0.1  $\mu\text{M}$  heme-conjugated recombinant HO-1 + 100  $\mu\text{M}$  compound **11**.

**Table 4:** Docking results from template docking

Ligand	MolDock score (a.u.)	Rerank score (a.u.)	Protein interaction (a.u.)	Cofactor interaction (a.u.)	Similarity score (a.u.)
<b>13</b>	-110.693	-67.1978	-67.556	-35.817	-371.011
<b>11</b>	-108.32	-70.3848	-63.481	-39.826	-359.656
<b>8</b>	-107.097	-65.4958	-63.925	-41.635	-384.167
<b>10S</b>	-88.1562	-60.4809	-57.173	-30.143	-383.821
<b>10R</b>	-85.1569	-59.4934	-61.203	-23.752	-375.972
<b>3</b>	-84.6499	-59.188	-58.274	-37.300	-449.158
<b>12</b>	-84.3847	-59.665	-49.600	-32.329	-380.361
<b>9</b>	-75.9043	-50.6081	-45.629	-31.596	-380.616

a.u., arbitrary units.

threshold value  $-500$  as expected with a RMSD of  $1.6 \text{ \AA}$  (Figure 11A). Typically, a RMSD value below  $2.0 \text{ \AA}$  represents a good solution for a redocked ligand, considering possible deviations coming out from rotatable bonds. The redocked compound **3** also formed an additional H-bond with Asp140 residue (Figure 11B), as reported by Rahman *et al.* (33).

Compound **11** is a very good ligand in terms of both MolDock score and reranking score (Table 4, Figure 12). The N-3 imidazole average distance of the active compounds from the iron(II) ranges around

$2.6 \text{ \AA}$ , a value still comparable with  $2.1 \text{ \AA}$  suggested by the crystallographic compound **3** structure. All the ligands interact with the same residues of the target protein: Arg136, Asp140, Gly139, forming a hydrophilic patch; Met34, Phe37, Leu54, Leu167, Leu147, characterizing the hydrophobic pocket. Compound **11** forms H-bond with Arg136.

Docking cannot exactly reproduce the binding process above all ligands when metal coordination is involved. The anchorage might also counteract the desolvation's effect, which is the dominant one in the binding process. Compound **13** possessing an experimental  $\text{IC}_{50} > 100 \mu\text{M}$  was also included in the dataset as a decoy to negatively validate the inhibition mechanism. Compound **13** shows a very good interaction with HO-1 (Table 4, Figure 13) in comparison with the other ligands. Using the Data Analyzer Tool of MVD, it was also possible to align molecules and extract detailed information about the similarity based on the overlap from each individual template point. The best scoring poses of the ligands were tested. Compound **13** gave a good normalized value for steric groups (Table 5). The steric group is used to shape matching without taking any chemical properties into account.

Standard semi-flexible docking and flexible docking were also carried out. In these two approaches, the ligands are not constrained to assume conformation similar to compound **3** one in 3CZY. A lower correlation grade with the experimental data was found.

**Figure 11:** (A) Compound **3** (thin sticks) in a complex with HO-1. (B) Compound **3** best pose (thin sticks) from *template docking* calculations. The H-bond between compound **3** and Asp140 is shown through the green dash.

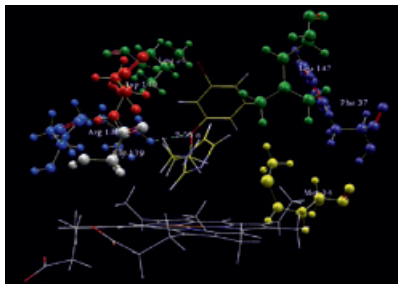
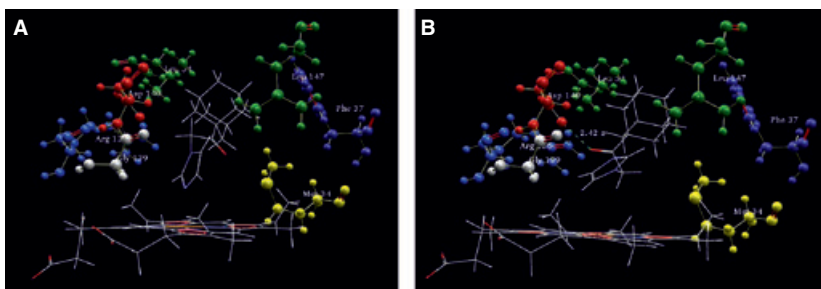


**Figure 12:** Compound **11** (yellow lines) best pose from *template docking* calculations. H-bond between ether oxygen and Arg136 is shown through the green dashes.

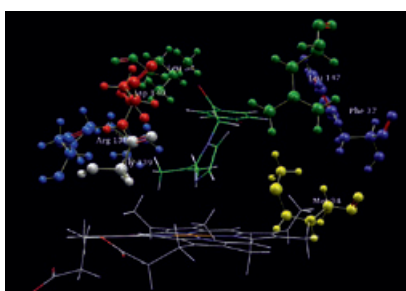


**Figure 13:** Compound **13** best pose (green lines) from *template docking* calculations.

**Table 5:** Atom matching values of best score poses to steric groups of template. The standard deviation is 0.053

Ligand	Overall steric group matching
<b>8</b>	0.864
<b>9</b>	0.793
<b>10S</b>	0.813
<b>11</b>	0.727
<b>12</b>	0.797
<b>13</b>	0.807
<b>3</b>	0.910

As predicted by the flexible docking, the 2-isopropyl substituent on the imidazole (compound **13**) points to a hydrophobic region of the binding pocket and forces the molecule to an alternate counterproductive binding mode, while the 4-bromophenyl group poses closer to the heme group (Figure 14). Therefore, the imidazolyl group of

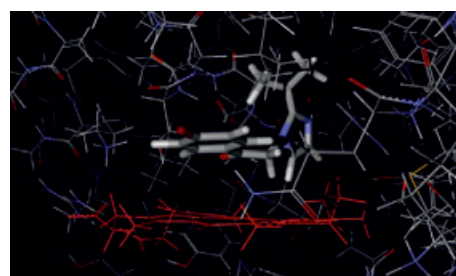


**Figure 14:** Compound **13** best pose from flexible docking.

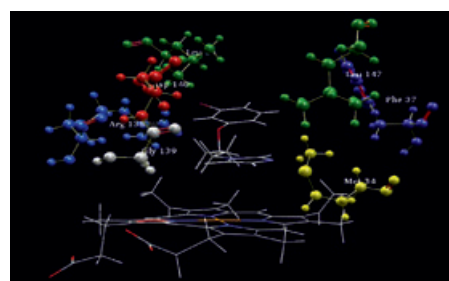


**Figure 15:** Compound **11** best pose (thin sticks) from standard semi-flexible docking.

**13** cannot co-ordinate the iron (II) ion by the N-3 nitrogen so the anchorage of the ligand to a key element of the catalytic site is lost, justifying the inactivity of **13** and supporting the mechanism of action and the hypothesis underlying the compounds selection. It must be considered a *false-positive* result: this might happen when the ranking compounds, referred to the docking energy scores, show the highly ranked ones (no perfect ranking scheme exists).

All HO-1 ligands in these calculations interact with heme by  $\pi$ - $\pi$  stacking 'ferrocene-like' interactions; as an example, Figure 15 shows compound **11** best pose from semi-flexible docking. An off-centered parallel orientation was found.

With flexible docking studies, it has been possible to dock the ligands considering the effective flexibility of the residues involved in the binding process. The correlation with the experimental data was not bad, but sometimes, using side-chain flexibility of the residues, the cavity site can become too big and the smoothing of the potential energy might generate the loss of some important interactions with the key residues. The reason for the better correlation

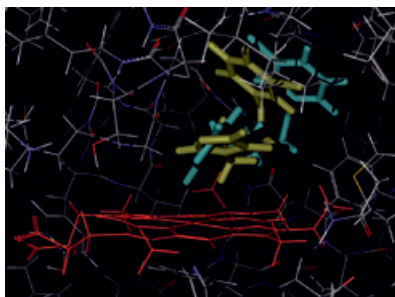


**Figure 16:** Compound **11** best pose (cyan lines) from template docking and best pose (dark yellow lines) from flexible docking.

with the experimental inhibition data using the template docking option is most likely due to the use of a template, which dictates to some degree the docking simulation. This might outweigh, to some extent, possible alternate binding conformations in the active ligands, as for the above-mentioned 'ferrocene-like' mechanism. Compound **11** best pose from the flexible docking shows a binding mode quite similar to the template docking one as depicted in Figure 16. All the MVD protocols and docking by alternate softwares (data not shown) failed to rationalize the activity of compound **12** for which additional data by experimental mechanistic and molecular dynamics (MD) studies need (57).

## Conclusions and Future Directions

HO-1 inhibition of a set of imidazole-based compounds (**8–13**), which contain the imidazole as a common core but differ in side-chain substitution, was reported. Obtained data revealed general good inhibition of HO-1 derived from rat spleen microsomal fractions. Compound **11**, which possesses a 3-bromophenoxybutyl chain, was found as a quite potent inhibitor ( $IC_{50} = 2.1 \mu M$ ). Moreover, compound **11** was able to form a complex with heme bound to recombinant hHO-1 at low micromolar concentrations. This could justify its selectivity versus HO-1 rather than other heme enzymes such as NOS or CYP450. Docking studies proved the existence of diverse binding modes for various compounds: the imidazole interaction with the heme iron is likely to be a fundamental determinant of the difference in the binding. Docking results were in good agreement both with experimental data and the built structure-based pharmacophoric model, which might be useful to design novel potential HO-1 inhibitors. Future studies aiming to better define the SARs, also by scaffold hopping to replace the *multi-tasking* imidazole ring, are in progress. Our results support the potential role of the subject compounds as pharmacological tools to elucidate the physiological functions of HO-1; selective compounds might be also taken into account for therapeutic applications.

## Acknowledgments

The authors thank Inte:ligand (Clemens-Maria Hofbauer-G. 6 2344 Maria Enzersdorf Austria/Europe; Mariahilferstraße 74B/11 1070 Wien/Vienna) for the software LIGANDSCOUT 3.0. and Dr Renè Thomsen (Molegro ApS, Denmark) for technical support and the helpful suggestions.

## References

1. Tenhunen R., Marver H.S., Schmid R. (1968) The enzymatic conversion of heme to bilirubin by microsomal heme oxygenase. *Proc Natl Acad Sci USA*;61:748–755.
2. Snyder S.H., Baranano D.E. (2001) Heme oxygenase: a font with multiple messengers. *Neuropsychopharmacology*;25:294–298.
3. De Matteis F., Dawson S.J., Pons N., Pipino S. (2002) Bilirubin and uroporphyrinogen oxidation by induced cytochrome P4501A and cytochrome P4502B: role of polyhalogenated biphenyls of different configuration. *Biochem Pharmacol*;63:615–624.
4. Maines M.D. (1988) Heme oxygenase: function, multiplicity, regulatory mechanisms, and clinical applications. *FASEB J*;2:2557–2568.
5. McCoubrey W.K., Huang T.J., Maines M.D. (1997) Isolation and characterization of a cDNA from the rat brain that encodes hemoprotein heme oxygenase-3. *Eur J Biochem*;247:725–732.
6. Ryter S.W., Alam J., Choi A.M. (2006) Heme oxygenase-1/carbon monoxide: from basic science to therapeutic applications. *Physiol Rev*;86:583–650.
7. Lee T.S., Chau L.Y. (2002) Heme oxygenase-1 mediates the anti-inflammatory effect of interleukin-10 in mice. *Nat Med*;8:240–246.
8. Lee T.S., Tsai H.L., Chau L.Y. (2003) Induction of heme oxygenase-1 expression in murine macrophages is essential for the anti-inflammatory effect of low dose 15-deoxy-delta 12,14-prostaglandin J2. *J Biol Chem*;278:19325–19330.
9. Imuta N., Hori O., Kitao Y., Tabata Y., Yoshimoto T., Matsuyama T., Ogawa S. (2007) Hypoxia-mediated induction of heme oxygenase type I and carbon monoxide release from astrocytes protects nearby cerebral neurons from hypoxia-mediated apoptosis. *Antioxid Redox Signal*;9:543–552.
10. Deininger M.H., Meyermann R., Trautmann K., Duffner F., Grote E.H., Wickboldt J., Schluessener H.J. (2000) Heme oxygenase (HO)-1 expressing macrophages/microglial cells accumulate during oligodendroglioma progression. *Brain Res*;882:1–8.
11. McAllister S.C., Hansen S.G., Ruhl R.A., Raggo C.M., DeFilippis V.R., Greenspan D., Fruh K., Moses A.V. (2004) Kaposi sarcoma-associated herpes virus (KSHV) induces heme oxygenase-1 expression and activity in KSHV-infected endothelial cells. *Blood*;103:3465–3473.
12. Tsuji M.H., Yanagawa T., Iwasa S., Tabuchi K., Onizawa K., Bannai S., Toyooka H., Yoshida H. (1999) Heme oxygenase-1 expression in oral squamous cell carcinoma as involved in lymphnode metastasis. *Cancer Lett*;138:53–59.
13. Berberat P.O., Dambrauskas Z., Gulbinas A., Giese T., Giese N., Kunzli B., Autschbach F., Meuer S., Buchler M.W., Friess H. (2005) Inhibition of heme oxygenase-1 increases responsiveness of pancreatic cancer cells to anticancer treatment. *Clin Cancer Res*;11:3790–3798.
14. Fang J., Akaike T., Maeda H. (2004) Antiapoptotic role of heme oxygenase (HO) and the potential of HO as a target in anticancer treatment. *Apoptosis*;9:27–35.
15. Mayerhofer M., Florian S., Krauth M.T., Aichberger K.J., Bilban M., Marculescu R., Printz D., Fritsch G., Wagner O., Selzer E., Sperr W.R., Valent P., Sillaber C. (2004) Identification of heme oxygenase-1 as a novel BCR/ABL-dependent survival factor in chronic myeloid leukemia. *Cancer Res*;64:3148–3154.

16. Fang J., Sawa T., Akaike T., Greish K., Maeda H. (2004) Enhancement of chemotherapeutic response of tumor cells by a heme oxygenase inhibitor, pegylated zinc protoporphyrin. *Int J Cancer*;109:1–8.
17. Nowis D., Legat M., Grzela T., Niderla J., Wilczek E., Wilczynski G.M., Glodkowska E. *et al.* (2006) Heme oxygenase-1 protects tumor cells against photodynamic therapy-mediated cytotoxicity. *Oncogene*;25:3365–3374.
18. Was H., Cichon T., Smolarczyk R., Rudnicka D., Stopa M., Chevalier C., Leger J.J., Lackowska B., Grochot A., Bojkowska K., Ratajska A., Kieda C., Szala S., Dulak J., Jozkowicz A. (2006) Overexpression of heme oxygenase-1 in murine melanoma: increased proliferation and viability of tumor cells, decreased survival of mice. *Am J Pathol*;169:2181–2198.
19. Johnson R.A., Colombari E., Colombari D.S., Lavesa M., Talman W.T., Nasjletti A. (1997) Role of endogenous carbon monoxide in central regulation of arterial pressure. *Hypertension*;30:962–967.
20. Tulis D.A., Durante W., Peyton K.J., Evans A.J., Schafer A.I. (2001) Heme oxygenase-1 attenuates vascular remodeling following balloon injury in rat carotid arteries. *Atherosclerosis*;155:113–122.
21. Doi K., Akaike T., Fujii S., Tanaka S., Ikebe N., Beppu T., Shibahara S., Ogawa M., Maeda H. (1999) Induction of haem oxygenase-1, nitric oxide and ischaemia in experimental solid tumours and implications for tumour growth. *Br J Cancer*;80:1945–1954.
22. Fang J., Sawa T., Akaike T., Akuta T., Sahoo S.K., Khaled G., Hamada A., Maeda H. (2003) In vivo antitumor activity of pegylated zinc protoporphyrin: targeted inhibition of heme oxygenase in solid tumor. *Cancer Res*;63:3567–3574.
23. Hirai K., Sasahira T., Ohmori H., Fujii K., Kuniyasu H. (2007) Inhibition of heme oxygenase-1 by zinc protoporphyrin IX reduces tumor growth of LL/2 lung cancer in C57BL mice. *Int J Cancer*;120:500–505.
24. Luo D., Vincent S.R. (1994) Metalloporphyrins inhibit nitric oxide dependent cGMP formation in vivo. *Eur J Pharmacol*;267:263–267.
25. Meffert M.K., Haley J.E., Schuman E.M., Schulman H., Madison D.V. (1994) Inhibition of hippocampal heme oxygenase, nitric oxide synthase, and long-term potentiation by metalloporphyrins. *Neuron*;13:1225–1233.
26. Vlahakis J.Z., Kinobe R.T., Bowers R.J., Brien J.F., Nakatsub K., Szarek W.A. (2005) Synthesis and evaluation of azalanstat analogues as heme oxygenase inhibitors. *Bioorg Med Chem Lett*;15:1457–1461.
27. Vlahakis J.Z., Kinobe R.T., Bowers R.J., Brien J.F., Nakatsu K., Szarek W.A. (2006) Imidazole-Dioxolane Compounds as Isozyme-Selective Heme Oxygenase Inhibitors. *J Med Chem*;49:4437–4441.
28. Vlahakis J.Z., Humb M., Rahman M.N., Jia Z., Nakatsu K., Szarek W.A. (2009) Synthesis and evaluation of imidazole-dioxolane compounds as selective heme oxygenase inhibitors: effect of substituents at the 4-position of the dioxolane ring. *Bioorg Med Chem*;17:2461–2475.
29. Roman G., Riley J.G., Vlahakis J.Z., Kinobe R.T., Brien J.F., Nakatsub K., Szarek W.A. (2007) Heme oxygenase inhibition by 2-oxy-substituted 1-(1H-imidazol-1-yl)-4-phenylbutanes: effect of halogen substitution in the phenyl ring. *Bioorg Med Chem*;15:3225–3234.
30. Roman G., Vlahakis J.Z., Vukomanovic D., Nakatsu K., Szarek W.A. (2010) Heme oxygenase inhibition by 1-Aryl-2-(1H-imidazol-1-yl/1H-1,2,4-triazol-1-yl) ethanones and their derivatives. *Chem Med Chem*;5:1541–1555.
31. Kinobe R.T., Vlahakis J.Z., Vreman H.J., Stevenson D.K., Brien J.F., Szarek W.A., Nakatsu K. (2006) Selectivity of imidazole-dioxolane compounds for in vitro inhibition of microsomal haem oxygenase isoforms. *Br J Pharmacol*;147:307–315.
32. Rahman M.N., Vlahakis J.Z., Szarek W.A., Nakatsu K., Jia Z. (2008) X-ray crystal structure of human heme oxygenase-1 in complex with 1-(Adamantan-1-yl)-2-(1H-imidazol-1-yl)ethanone: a common binding mode for imidazole-based heme oxygenase-1 inhibitors. *J Med Chem*;51:5943–5952.
33. Rahman M.N., Vlahakis J.Z., Roman G., Vukomanovic D., Szarek W.A., Nakatsu K., Jia Z. (2010) Structural characterization of human heme oxygenase-1 in complex with azole-based inhibitors. *J Inorg Biochem*;104:324–330.
34. Huber W.J. III, Backes W.L. (2007) Expression and characterization of full-length human heme oxygenase-1: the presence of intact membrane-binding region leads to increased binding affinity for NADPH cytochrome P450 reductase. *Biochemistry*;46:12212–12219.
35. Huber W.J. III, Scruggs B.A., Backes W.L. (2009) C-Terminal membrane spanning region of human heme oxygenase-1 mediates a time-dependent complex formation with cytochrome P450 reductase. *Biochemistry*;48:190–197.
36. Huber W.J. III, Marohnic C.C., Peters M., Alam J., Reed J.R., Masters B.S. (2009) Measurement of membrane-bound human heme oxygenase-1 activity using a chemically defined assay system. *Drug Metab Dispos*;37:857–864.
37. Salerno L., Sorrenti V., Guerrera F., Sarvà M.C., Siracusa M.A., Di Giacomo C., Vanella A. (1999) N-substituted-imidazoles as inhibitors of nitric oxide synthase: a preliminary screening. *Pharmazie*;54:685–690.
38. Salerno L., Sorrenti V., Guerrera F., Sarvà M.C., Siracusa M.A., Di Giacomo C., Vanella A. (1999) 1-[(aryloxy)alkyl]-1H-imidazoles as inhibitors of neuronal nitric oxide synthase. *Pharm Pharmacol Commun*;5:491–494.
39. Sorrenti V., Di Giacomo C., Salerno L., Siracusa M.A., Guerrera F., Vanella A. (2001) Inhibition of neuronal nitric oxide synthase by N-phenacyl imidazoles. *Nitric Oxide*;5:32–38.
40. Di Giacomo C., Sorrenti V., Salerno L., Cardile V., Guerrera F., Siracusa M.A., Avitabile M., Vanella A. (2003) Novel inhibitors of neuronal nitric oxide synthase. *Exp Biol Med*;228:486–490.
41. Sorrenti V., Salerno L., Di Giacomo C., Acquaviva R., Siracusa M.A., Vanella A. (2006) Imidazole derivatives as antioxidants and selective inhibitors of nNOS. *Nitric Oxide*;14:45–60.
42. Salerno L., Modica M.N., Romeo G., Pittalà V., Siracusa M.A., Amato M.E., Acquaviva R., Di Giacomo C., Sorrenti V. (2012) Novel inhibitors of nitric oxide synthase with antioxidant properties. *Eur J Med Chem*;49:118–126.
43. Xia Z.W., Cui W.J., Zhang X.H., Shen Q.X., Wang J., Li Y.Z., Chen S.N., Yu S.C. (2002) Analysis of heme oxygenase isomers in rat. *World J Gastroenterol*;8:1123–1128.
44. Trakshel G.M., Kutty R.K., Maines M.D. (1988) Resolution of the rat brain heme oxygenase activity: absence of a detectable amount of the inducible form (HO-1). *Arch Biochem Biophys*;260:732–739.

45. Ryter S.W., Kvam E., Tyrrell R.M. (2000) Heme oxygenase activity. Current methods and applications. *Methods Mol Biol*;99:369–391.
46. Lowry O.H., Rosenbrough N.J., Farr A.J., Randall R.G. (1951) Protein measurement with the Folin phenol reagent. *J Biol Chem*;193:265–275.
47. Kinobe R.T., Dercho R.A., Vlahakis J.Z., Brien J.F., Szarek W.A., Nakatsu K. (2006) Inhibition of the enzymatic activity of heme oxygenases by azole-based antifungal drugs. *J Pharmacol Exp Ther*;319:277–284.
48. Beaven G.H., Chen S.H., d'Albis A., Gratzner W.B. (1974) A spectroscopic study of the haemin–human-serum-albumin system. *Eur J Biochem*;41:539–546.
49. Collier G.S., Pratt J.M., De Wet C.R., Tshabalala C.F. (1979) Studies on haemin in dimethyl sulphoxide/water mixture. *Biochem J*;179:281–289.
50. Thomsen R., Christensen M.H. (2006) MolDock: a new technique for high-accuracy molecular docking. *J Med Chem*;49:3315–3321.
51. Schüttelkopf W., van Aalten D.M.F. (2004) PRODRG -a tool for high-throughput crystallography of protein-ligand complexes. *Acta Crystallogr*;60:1355–1363.
52. Wolber G., Langer T. (2005) LigandScout:3-D pharmacophores derived from protein-bound ligands and their use as virtual screening filters. *J Chem Inf Comput Sci*;45:160–169.
53. Halgren T.A. (1996) Merck molecular force field. V. Extension of MMFF94 using experimental data, additional computational data and empirical rules. *J Comp Chem*;17:616–641.
54. Vlahakis J.Z., Rahman M.N., Roman G., Jia Z., Nakatsu K., Szarek W.A. (2011) Rapid, convenient method for screening imidazole-containing compounds for heme oxygenase inhibition. *J Pharmacol Toxicol Methods*;63:79–88.
55. Hu H.B., Wang W., Han L., Zhou W.P., Zhang X.H. (2007) An improved method for purification of recombinant truncated heme oxygenase-1 by expanded bed adsorption and gel filtration. *Bioprocess Biosyst Eng*;30:87–90.
56. Vukomanovic D., McLaughlin B., Rahman M.N., Vlahakis J.Z., Roman G., Dercho R.A., Kinobe R.T., Hum M., Brien J.F., Jia Z., Szarek W.A., Nakatsu K. (2010) Recombinant truncated and microsomal heme oxygenase-1 and -2: differential sensitivity to inhibitors. *Can J Physiol Pharmacol*;88:480–486.
57. Rohrig U.F., Grosdidier A., Zoete V., Michielin O. (2009) Docking to heme proteins. *J Comput Chem*;30:2305–2315.

## Note

<sup>a</sup>Molegro ApS, Aarhus C, Denmark.